Exchange bias and its thermal stability in ferromagnetic/antiferromagnetic antidot arrays

W. J. Gong, W. J. Yu, W. Liu, S. Guo, S. Ma et al.

Related Articles

Effect of thermal cycle on the interfacial antiferromagnetic spin configuration and exchange bias in Ni-Mn-Sb alloy
AIP Advances 2, 032181 (2012)

Exchange bias coupling of Co with ultrathin La2/3Sr1/3MnO3 films
Appl. Phys. Lett. 101, 122409 (2012)

Ruderman-Kittel-Kasuya-Yosida interaction between diluted magnetic semiconductor quantum dots embedded in semiconductor
J. Appl. Phys. 112, 063905 (2012)

High temperature phase transformation studies in magnetite nanoparticles doped with Co2+ ion
J. Appl. Phys. 112, 054320 (2012)

Positive and negative exchange bias effects in the simple perovskite manganite NdMnO3
Appl. Phys. Lett. 101, 102411 (2012)

Additional information on Appl. Phys. Lett.

Journal Homepage: http://apl.aip.org/
Journal Information: http://apl.aip.org/about/about_the_journal
Top downloads: http://apl.aip.org/features/most_downloaded
Information for Authors: http://apl.aip.org/authors

Exchange bias and its thermal stability in ferromagnetic/antiferromagnetic antidot arrays

W. J. Gong, W. J. Yu, W. Liu,[a] S. Guo, S. Ma, J. N. Feng, B. Li, and Z. D. Zhang
Shenyang National Laboratory for Materials Science and International Centre for Materials Physics, Institute of Metal Research, Chinese Academy of Sciences, Shenyang 110016, People's Republic of China

The exchange bias (EB) effect and its thermal stability in nanoscale Co/NiO antidot arrays and sheet films have been investigated. The EB field H_E increases with increasing Co thickness (t_{Co}) and reaches a maximum at $t_{Co} = 8$ nm in the antidot arrays, whereas H_E decreases with t_{Co} in the sheet films. Compared with the sheet films, H_E in the antidot arrays is either enhanced or decreased, depending on the thickness of the ferromagnetic Co layer, which is due to the three-dimensional effects in the antiferromagnetic NiO and ferromagnetic Co layers caused by the nanopores. A higher thermal stability is observed in the antidot arrays due to the out-of-plane anisotropy constant K_1 of the misaligned antiferromagnetic magnetization component. © *2012 American Institute of Physics*. [http://dx.doi.org/10.1063/1.4733341]

The exchange bias (EB) effect, originating from the interfacial coupling between ferromagnetic (FM) and antiferromagnetic (AFM) bilayers, has attracted considerable interest.[1] As the dimensions of nanostructured magnetic materials become comparable to their characteristic length scales (e.g., domain-wall width, exchange length), their magnetic properties will be different from sheet films.[2,3] Recently, there has been considerable interest in the EB effect of patterned magnetic nanostructures, because of the many applications in high-density magnetic recording, magnetic sensors, and magnetic random access memories.[4,5] Various routes, such as electron-beam lithography,[6] block copolymer templates,[7] and nanoporous ZrO_2 membranes,[8] have been used to fabricate patterned magnetic nanostructures. Among the various nanofabrication methods, an easy and low-cost way is to deposit magnetic materials onto porous anodic aluminum oxide (AAO) templates. It has been reported that for antidot arrays, which consist of an array of pores in the sheet EB films, the coercivity field H_C and the EB field H_E are enhanced.[9] However, also the opposite has been reported. It has been found that in CoFe/IrMn EB nanostructure, H_E can be either enhanced due to the pinning of AFM spins or suppressed because of the misalignment of AFM and FM spins at the edge of the pores, depending on the pore density.[10] In Co/CoO EB antidot arrays, a three-dimensional magnetization profile and multi-axes EB have been found due to the locally crescent shape of the Co films.[11]

In this work, we investigate influence of FM layer thickness and thermal-activation effects on EB phenomenon in Co/NiO antidot arrays and sheet films. It is found that the EB field H_E in the Co/NiO antidot arrays can be either larger or smaller than in the sheet films, depending on the FM thickness. In addition, the blocking temperature of the antidot arrays is higher than that of the sheet films. These results can be explained by an anisotropy distribution in the FM/AFM layer that has been modified by the membranes. This also explains the controversial previous reports on enhanced vs

decreased EB field and on the thermal stability of patterned nanostructures.

AAO templates with pore depth of $30\,\mu m$, Si(001), and Al_2O_3(0001) were used as substrates. Nanoporous AAO templates were made by anodizing high-purity aluminum foils in a two-step anodization process in a sulfuric acid solution.[12] Ag(10 nm)/Co(t_{Co})/NiO(5 nm)/Ag(5 nm) antidot arrays on AAO templates and the corresponding sheet films on Si and Al_2O_3 substrates were prepared by means of using DC and RF magnetron sputtering of Ag, Co, NiO targets with 99.99% purity.[13] The base pressure was better than 3×10^{-7} Torr and the Ar pressure during deposition was 4×10^{-3} Torr. The morphological characterization was carried out with high-resolution scanning electron microscopy (SEM) and Tecnai G^2 F20 transmission electron microscopy (TEM). The magnetic properties were measured at different temperatures after field cooling (FC) from 300 K in a field of 5 kOe in a superconducting quantum interference device (SQUID) magnetometer.

A SEM image of Ag(10 nm)/Co(8 nm)/NiO(5 nm)/Ag(5 nm) antidot arrays is shown in Fig. 1(a). The pore diameter is about 40 nm and the edge-to-edge spacing about 50 nm. Due to the high aspect ratio (pore depth/diameter), a sawtooth shape of the films is found. The cross-sectional TEM image in the inset of Fig. 1(a) shows that the materials are mainly on the top and the inner wall of the templates, and no materials reach the bottom of the pores. Figure 1(b) presents a three-dimensional sketch of the films deposited on top of the AAO templates. The direction of the FM and AFM moments at the edge and at the inner wall of the nanopores deviates from the in-plane direction.

The in-plane hysteresis loops at 10 K of Ag(10 nm)/Co(t_{Co})/NiO(5 nm)/Ag(5 nm) EB antidot arrays and sheet films on Si with $t_{Co} = 2, 3, 5, 8, 12, 15$ nm after FC are shown in Fig. 2. All hysteresis loops display a shift along the magnetic-field axis. The magnetization curves of the sheet films with $t_{Co} < 5$ nm reveal an asymmetric hysteresis loops and large loop shift. A small shoulder appears in the descending branch of the magnetization curves of the sheet
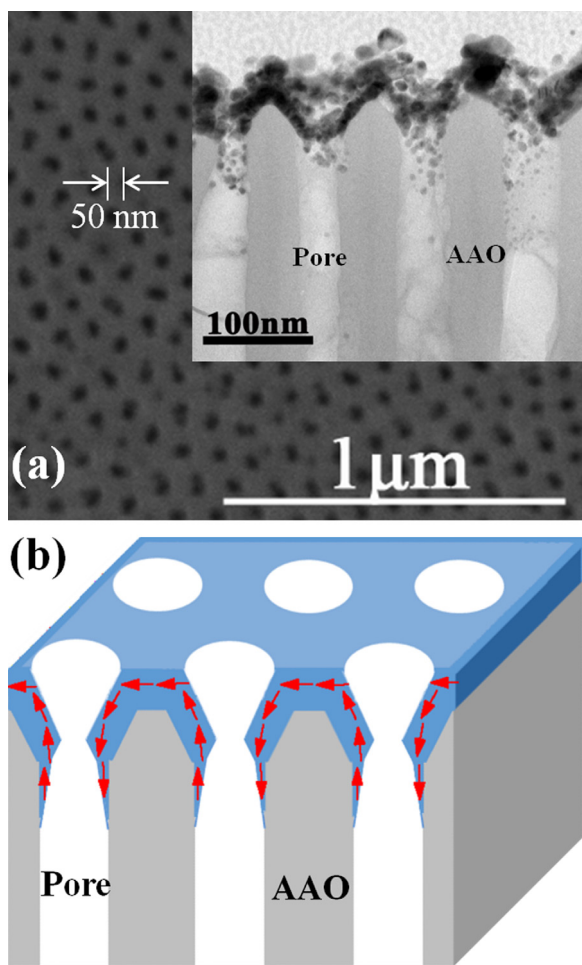
FIG. 1. (a) SEM image of Ag(10 nm)/Co(8 nm)/NiO(5 nm)/Ag(5 nm) antidot arrays. Inset: cross-sectional TEM image of the antidot arrays. (b) Three-dimensional sketch of the antidot arrays, the arrows indicate the magnetization direction of magnetic films at remanence.

FIG. 2. (a)-(f) In-plane hysteresis loops of Ag(10 nm)/Co(t_{Co})/NiO(5 nm)/Ag(5 nm) antidot arrays on AAO (solid squares) and sheet films on Si (open circles) with $t_{Co} = 1.5, 3, 5, 8, 12, 15$ nm. Inset in (a): the enlarged view of hysteresis loop of antidot arrays with $t_{Co} = 1.5$ nm. The two additional hysteresis loops in (d): out-of-plane hysteresis loops of antidot arrays (half-filled circle) and of sheet films on Si (open triangle).

films with $t_{Co} < 5$ nm, which may origin from the asymmetric magnetization reversal mechanism or reversal of a partly unbiased Co layer. For $t_{Co} = 1.5$ nm, a small coercivity field H_C of 0.32 kOe and EB field H_E of 0.15 kOe are observed in the antidot arrays. As shown in the inset in Fig. 2(a), irreversible magnetization hysteresis loop can be seen in the thin antidot arrays. As shown in Fig. 2(b)), a small loop shift and a two-step magnetization reversal process are observed in the antidot arrays with $t_{Co} = 3$ nm, which suggests a three-dimensional magnetization effects in the antidot arrays. Since no materials are found at the bottom of the pores, the formation of vortex state at the bottom of the pores is excluded. The hysteresis loops of the films with antidot arrays are canted and more asymmetric than the loops of the sheet films, which is another indication of three-dimensional magnetization effects in the films, similar to Cu/Co/Cu tri-layers deposited on nanoporous alumina membranes.[11] Moreover, the entrance of the pores may be filled in the antidot arrays with the thickest Co layer, which may also cause the similar hysteresis loops in antidot arrays and the sheet films with thick Co layer. Magnetic moments along the inner wall of the nanopores are aligned perpendicularly to the film plane, whereas the moments between the nanopores are aligned within the film plane, as sketched in Fig. 1(b).

The antidot arrays and the sheet films exhibit an interesting variation of H_C and H_E with t_{Co} (Fig. 3). For the sheet films, H_C and H_E decrease with t_{Co}, which is characteristic for EB sheet bilayers and thus suggests a mainly interfacial character of the FM-AFM coupling in the sheet films.[14] The substrates may affect Ag underlayer's texture slightly and modify the anisotropy of the magnetic layers, which may induce the differences between the amplitudes of H_C and H_E for the sheet films on Si and Al_2O_3 substrates with $t_{Co} < 5$ nm, whereas the effect is small for the sheet films on Si and Al_2O_3 substrates with thick t_{Co}. The larger H_C of the antidot arrays with $t_{Co} \geq 5$ nm compared with sheet films can be attributed to domain-wall pinning in the vicinity of the nanopores. The pinning centers, introduced by the presence of the nanopores, impede the domain-wall motion and increase H_C correspondingly, which has been confirmed by experiments and micromagnetic simulation.[15,16] The smaller H_C of the antidot arrays with $t_{Co} < 5$ nm may be caused by misaligned magnetic moments of the FM and AFM components at the edge of the nanopores. With increasing Co thickness, H_E of the antidot arrays increases, reaching a maximum at $t_{Co} = 8$ nm and then decreases with further increasing t_{Co}. In addition, for $t_{Co} > 5$ nm, H_E of the antidot arrays is larger than H_E of the sheet films, which is attributed to pinning in the antidot arrays.[17] Similar behavior of H_E is
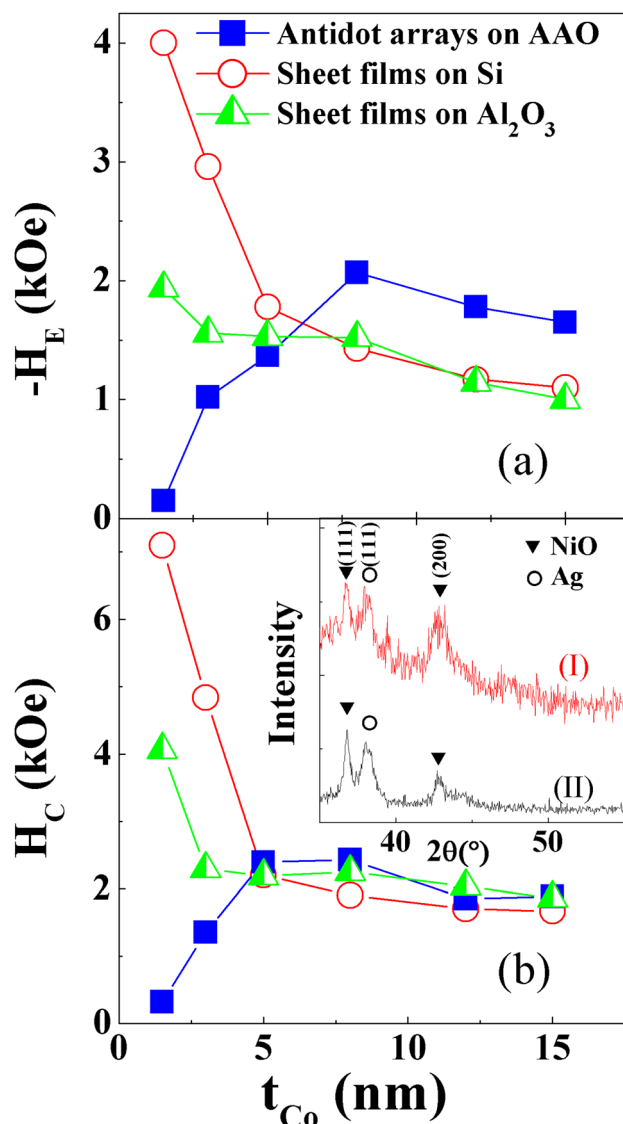
FIG. 3. Variation of H_E (a), H_C (b) with the Co thickness t_{Co} of antidot arrays on AAO (solid squares), of sheet films on Si and Al_2O_3 (open circles and triangles, respectively). Inset: XRD patterns of Ag(10 nm)/Co(8 nm)/NiO(5 nm)/Ag(5 nm) antidot arrays (I) and sheet films on Si (II).

observed in the sheet films on Si and on Al_2O_3 substrates, which means that different substrates are irrelevant to the origin of the different EB behaviors. The XRD results of the inset in Fig. 3(b) show the NiO (111) texture is observed in the antidot arrays and the sheet films. The spins of NiO show ferromagnetic order within the (111) plane while adjacent (111) planes are antiparallel aligned. Using values for the exchange stiffness $A_1 = 1.6 \times 10^{-7}$ erg/cm for the nearest neighbors and $A_2 = 6.7 \times 10^{-7}$ erg/cm for the next-nearest neighbors, and using the magnetic-anisotropy constants $K_1 = 2.9 \times 10^6$ erg/cm^3 perpendicular to the (111) plane and $K_2 = 1.5 \times 10^5$ erg/cm^3 parallel to the (111) plane,[18] the AF domain-wall width parallel to the (111) plane can be estimated to be $\delta_{AF} = \pi(A_2/K_2)^{1/2} = 66$ nm. The small nearest-neighbor exchange stiffness A_1 has been neglected in the calculation of the domain-wall width. When the films are deposited on the AAO templates, the nanopores reduce the domain size of NiO, which results in a larger interface exchange coupling. According to the random-field model,[19] the domain size is mainly determined by ferromagnetic

exchange interaction within the FM layer and the random field acting on the FM layer due to interfacial exchange coupling. In this static model, the exchange field is inversely proportional to the AF domain size. In the antidot arrays, the nanopores reduce the FM domain size more than in sheet films and also increase the random field, which is essential for an increased H_E. However, for the antidot arrays with $t_{Co} \leq 5$ nm, H_E is smaller than for the sheet films, which is attributed to the misalignment of FM and AFM spins at the edge and wall of the nanopores. The Co/NiO layers aligned along the inner wall in the antidot arrays have a perpendicular preferential orientation of magnetization. The slanter hysteresis loops for all antidot arrays and the step in the hysteresis loop for $t_{Co} = 3$ nm are indications of a special magnetization distribution in the antidot arrays. For both the sheet films and the antidot arrays with $t_{Co} = 8$ nm, the out-of-plane EB field H_E is smaller than the in-plane EB field H_E (Fig. 2). For small t_{Co}, more FM magnetic moments in the antidot arrays deviate from the in-plane direction, causing that H_E and H_C of the antidot arrays are smaller than of the sheet films.

To investigate the effects of thermal activation on the EB of the antidot arrays and the sheet films, the temperature dependence of H_E has been measured. Figure 4 shows the variation of H_E and H_C with temperature of the antidot arrays and sheet films. H_E and H_C decrease with increasing temperature because the thermal energy prevails over the exchange coupling between the AFM and FM layers. Interestingly, the blocking temperature (T_b, the temperature where the EB field completely disappears) of the antidot arrays is higher than of the sheet films on Si and Al_2O_3, which indicates a larger effect of thermal activation in the sheet films. It is clear from the inset in Fig. 4 that the blocking temperature varies with the pore diameter (d) and the higher blocking temperature is observed in the antidot arrays compared with sheet films,
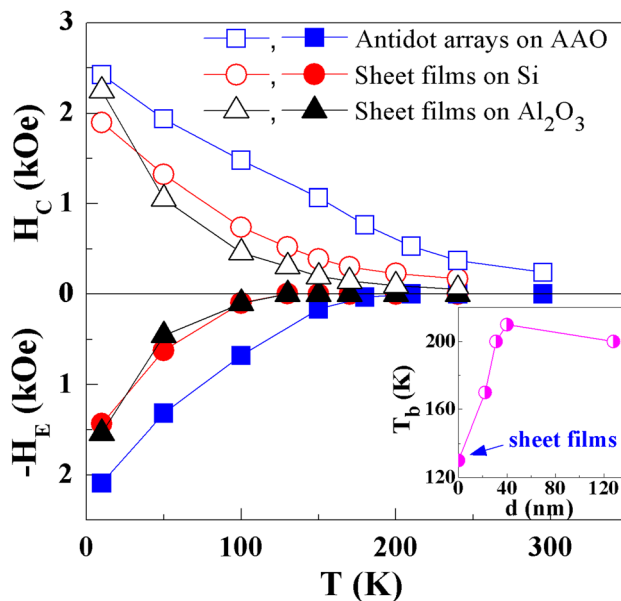
FIG. 4. Temperature dependence of H_E and H_C of Ag(10 nm)/Co(8 nm)/NiO(5 nm)/Ag(5 nm) antidot arrays with pore diameter of 40 nm (squares), and sheet films on Si and Al_2O_3 (circles and triangles). Inset: variation of T_b with pore diameters d for Ag(10 nm)/Co(8 nm)/NiO(5 nm)/Ag(5 nm) antidot arrays and for sheet films.

and the largest blocking temperature enhancement appears in the antidot arrays with $d = 40$ nm. In comparison with the antidot arrays with smaller diameter of pores, the decrease of quantity of the pores and ratio of materials on the wall/top of AAO templates in the antidot arrays with $d = 128$ nm may reduce the contribution of the perpendicular magnetization component, causing the decrease of T_b. This effect of thermal activation is more pronounced in the sheet films than in the antidot arrays, which has rarely been reported. In Co/CoO and [Co/Pd]$_n$/CoO antidot arrays, there exists a crossing temperature in the temperature dependence of H_E, leading to temperature ranges in which H_E for the antidot arrays can be either smaller or larger than in the sheet films.[3,20] This is attributed to a strong competition between constraints imposed on the AFM domain size by reduction of the lateral dimensions of the antidot arrays, which favor an enhancement of H_E, and thermal activation effects that favor a reduction of H_E in antidot arrays. However, H_E of the antidot arrays of the present results is larger than that of the sheet films at temperatures below the blocking temperature. The perpendicular magnetization component of the FM/AFM bilayers is attributed to the enhanced in-plane blocking temperature of the antidot arrays. The FM/AFM magnetization direction lies along the inner wall of the AAO, causing a perpendicular magnetization component. According to the random-field model for FM/AFM systems, the domain wall in the AFM layers plays an important role in the EB effect. The competition between the interfacial exchange-coupling energy and the AFM domain-wall energy breaks the AFM layer into multidomains.[19,21] According to the model, the EB field H_E is related to the energy stored in the AFM domain wall by $H_E \propto (A_{AF}K_{AF})^{1/2}$. Assuming that A_{AF} is not dependent on temperature and that $K_{AF} = K_{AF}(0)(1-T/T_N)^2$ for the cubic anisotropy of the AF layers, the model gives $H_E \propto \sqrt{A_{AF}K_{AF}(0)}(1 - T/T_N)$ for the temperature dependence of H_E. Substituting T_b for T_N results in $H_E \propto \sqrt{A_{AF}K_{AF}(0)}(1 - T/T_b)$. Taking into account both the out-of-plane and the in-plane anisotropy, the NiO domain-wall energy can be expressed by[18] $\sigma_{AF} = 2\sqrt{A_{AF}K_1}\cos\alpha + 2/3\sqrt{2A_{AF}K_2}\cos 6\beta$, where A_{AF} is the exchange stiffness, α the coherent angle out of NiO(111) plane, β the coherent rotation angle from the easy axis $[\bar{1}2\bar{1}]$ within NiO(111) plane. The temperature dependence of H_E can be expressed as $H_E \propto C^{(1)}(1 - T/T_b^{(1)})^{\gamma^{(1)}} + C^{(2)}(1 - T/T_b^{(2)})\gamma^{(2)}$,[22] where $(T_b^{(1)}, \gamma^{(1)})$ and $(T_b^{(2)}, \gamma^{(2)})$ are determined by the temperature dependence of K_1 and K_2, respectively, and $C^{(1)}$ and $C^{(2)}$ are constants. In the sheet films, the NiO domain-wall energy is dominated by the in-plane anisotropy constant K_2, while the out-of-plane anisotropy constant K_1 plays a minor role. The temperature dependence of H_E is mainly controlled by the temperature dependence of the in-plane anisotropy constant K_2. However, in antidot arrays, the out-of-plane anisotropy constant K_1 plays a more important role due to the misaligned magnetic moments at the edge and at the inner wall of the nanopores. The much larger K_1 leads to a higher blocking temperature

T_b in the antidot arrays than in the sheet films. The higher blocking temperature in the antidot arrays, indicating an excellent thermal stability of these nanostructures, is attractive for modern spintronics applications.

In conclusion, we have studied the EB effect in Co/NiO antidot arrays and sheet films. The largest H_E of the antidot arrays is observed at $t_{Co} = 8$ nm. Compared with the sheet films, H_E of the antidot arrays can be enhanced or decreased by varying the thickness of Co layer, which is due to the misalignment of the FM and AFM layers at the edge and at the inner wall of the nanopores. The antidot arrays have excellent thermal stability for application in spintronics devices. The obtained results explain the controversial reports in literature[9–11] on the behavior of the EB field and its thermal stability in patterned nanostructures.

[1]J. Nogues and I. K. Schuller, J. Magn. Magn. Mater. **192**, 203 (1999).
[2]K. Liu, S. M. Baker, M. Tuominen, T. P. Russell, and I. K. Schuller, Phys. Rev. B **63**, 060403 (2001).
[3]A. O. Adeyeye and D. Tripathy, Phys. Rev. B **79**, 064413 (2009).
[4]J. Nogues, J. Sort, V. Langlais, V. Skumryev, S. Surinach, J. S. Munoz, and M. D. Baro, Phys. Rep. **422**, 65 (2005).
[5]O. Hellwig, T. Hauet, T. Thomson, E. Dobisz, J. D. Risner-Jamtgaard, D. Yaney, B. D. Terris, and E. E. Fullerton, Appl. Phys. Lett. **95**, 232505 (2009).
[6]A. O. Adeyeye, J. A. C. Bland, and C. Daboo, Appl. Phys. Lett. **70**, 3164 (1997).
[7]V. P. Chuang, W. Jung, C. A. Ross, J. Y. Cheng, O. H. Park, and H. C. Kim, J. Appl. Phys. **103**, 074307 (2008).
[8]C. Schulze, M. Faustini, J. Lee, H. Schletter, M. U. Lutz, P. Krone, M. Gass, K. Sader, A. L. Bleloch, M. Hietschold, M. Fuger, D. Suess, J. Fidler, U. Wolff, V. Neu, D. Grosso, D. Makarov, and M. Albrecht, Nanotechnology **21**, 495701 (2010).
[9]D. Tripathy, A. O. Adeyeye, and N. Singh, Appl. Phys. Lett. **93**, 022502 (2008).
[10]M. T. Rahman, N. N. Shams, D. S. Wang, and C. H. Lai, Appl. Phys. Lett. **94**, 082503 (2009).
[11]F. Fettar, L. Cagnon, and N. Rougemaille, Appl. Phys. Lett. **97**, 192502 (2010).
[12]A. P. Li, F. Muller, A. Birner, K. Nielsch, and U. Gosele, J. Appl. Phys. **84**, 6023 (1998).
[13]W. J. Gong, W. Liu, X. H. Liu, S. Guo, J. N. Feng, B. Li, and Z. D. Zhang, J. Appl. Phys. **109**, 043906 (2011).
[14]K. O'Grady, L. E. Fernandez-Outon, and G. Vallejo-Fernandez, J. Magn. Magn. Mater. **322**, 883 (2010).
[15]D. Suess, J. Fidler, K. Porath, T. Schrefl, and D. Weller, J. Appl. Phys. **99**, 08G905 (2006).
[16]M. T. Rahman, N. N. Shams, C. H. Lai, J. Fidler, and D. Suess, Phys. Rev. B **81**, 014418 (2010).
[17]V. Baltz, J. Sort, S. Landis, B. Rodmacq, and B. Dieny, Phys. Rev. Lett. **94**, 117201 (2005).
[18]H. Matsuyama, C. Haginoya, and K. Koike, Phys. Rev. Lett. **85**, 646 (2000).
[19]A. P. Malozemoff, Phys. Rev. B **35**, 3679 (1987).
[20]V. Baltz, J. Sort, B. Rodmacq, B. Dieny, and S. Landis, Phys. Rev. B **72**, 104419 (2005).
[21]Z. J. Li and S. F. Zhang, Appl. Phys. Lett. **77**, 423 (2000).
[22]Z. Y. Liu and S. Adenwalla, J. Appl. Phys. **94**, 1105 (2003).